Chemisorption of Pentacene on Pt(111) with a Little Molecular Distortion

Aldo Ugolotti,[*,†] Shashank S. Harivyasi,[‡] Anu Baby,[†] Marcos Dominguez,[¶,§] Anna Lisa Pinardi,[‖] Maria Francisca López,[‖] José Ángel Martín-Gago,[‖] Guido Fratesi,[⊥] Luca Floreano,[*,¶] and Gian Paolo Brivio[†]

†*Dipartimento di Scienze dei Materiali, Università degli Studi di Milano-Bicocca, via Cozzi 55, 20125, Milano, Italy*

‡*Institute of Solid State Physics, NAWI Graz, Graz University of Technology, Petersgasse 16, 8010 Graz, Austria*

¶*CNR-IOM, Laboratorio TASC, Basovizza SS-14, km 163.5, I-34149, Trieste, Italy*

§*Dipartimento di Fisica, Università degli Studi di Trieste, via Valerio 2, 34127, Trieste, Italy*

‖*Materials Science Factory, Instituto de Ciencia de Materiales de Madrid (ICMM-CSIC), Sor Juana Inés de la Cruz 3, E-28049 Madrid, Spain*

⊥*Dipartimento di Fisica, Università degli Studi di Milano, via Celoria 16, 20133, Milano, Italy*

E-mail: a.ugolotti@campus.unimib.it; floreano@iom.cnr.it

Abstract

We investigated the adsorption of pentacene on the (111) surface of platinum, which is an archetypal system for a junction with a low charge-injection barrier. We probed the structural and electronic configurations of pentacene by scanning tunnelling microscopy (STM), X-ray photoemission spectroscopy (XPS) and near-edge X-ray absorption fine structure (NEXAFS) spectroscopy measurements. We simulated the interface by means of *ab initio* methods based on the density functional theory (DFT) framework, while including the dispersion forces. We found that the molecules adsorb at the bridge site of the close-compact atom rows with the long axis parallel to the substrate's <110> directions, in a slightly distorted geometry, driven by the good match between the position of carbon atoms of the molecule and the underlying lattice of the surface. Most importantly, a chemical bond is formed at the interface which we attribute to the high chemical reactivity of the Pt substrate.

Introduction

Polyconjugated aromatic hydrocarbons (PAH) have emerged in the last decades as promising building blocks for active or injecting layers in opto-electronic devices[1,2] like organic light emitting diodes (OLEDs) and organic thin-film transistors (OTFTs).[3] One of the major reasons for interest in organic compounds is the availability of a large number of techniques to synthesize and grow these materials, which allows production of devices with novel properties and lower costs than those based on traditional inorganic semiconductors.[4,5] The molecular structure and the corresponding electronic properties of its layer in contact with the metal deeply influence the performance of such a device.[6] Therefore characterisation of that interface becomes of paramount importance since is the starting point for the growth of subsequent organic layers. PAHs are a prototype of π-conjugated systems and, among them, the pentacene (Pc, $C_{24}H_{12}$) and its derivatives are widely employed in organic electronics,[2,3] thanks to their high charge-carrier mobility.[2,6] Platinum (Pt) is often used in electronic devices as a high work function electrode and it may be coupled with Pc, which has a similar value for ionization potential.[5,6] This interface would act like a junction with a low charge-injection barrier and in the last few years OTFTs having the Pc/Pt junction have already been reported.[7,8] Moreover, Pt is also a well known ingredient for catalysis, thanks to its unfilled *d* and *s* bands.[9] Because of this property the interaction with Pt substrate is expected to be substantially stronger than with other metals, such as gold or silver. From an atomistic point of view, such a hybrid system is interesting since a significant part of the interaction between the atoms is due to long-range dispersion forces.[10] Density functional theory (DFT)[11,12] framework has become the standard for performing *ab initio* simulations, but its commonly employed exchange-correlation functionals do not account for dispersion forces. Introducing van der Waals (vdW) interaction into the DFT framework is still an active research field because a single method that provides an effective description for the diverse systems is still missing. Many approaches are available and choosing between them depends, among other factors, on the computational methods used and the level of accuracy needed.

In the literature benzene (Bz), being the smallest aromatic molecule, has been taken as a prototype to investigate metal-molecule interfaces. Its geometries and energies, while ad-

sorbed onto different metals, have been simulated and measured thoroughly.[13–17] The results show the relevance of the dispersion forces but unfortunately any relevant distortion of the molecule is not likely to be observed. Structural and morphological studies of thin Pc films have been reported for most of the coinage metal surfaces, where a large variety of different phases have been observed, according to the degree of molecule to substrate interaction.[18–21] In the case of gold and silver, Pc displays a weak interaction coupling with the substrate, whereas the degree of intermolecular interaction, as tailored by the molecular coverage, leads to the formation of different phases during the growth of the first two layers.[20,22–25] Only in the specific case of the reconstructed (1x2)-Au(110) surface, the substrate anisotropy effectively drives a more complex phase diagram for a few layers thickness.[18,26] A much stronger interaction has been reported for the case of Cu surfaces, where the molecular distortion is driven by chemisorption into a slightly bent configuration and is accompanied by vertical displacement (buckling) of the substrate atoms.[27] As a result of chemisorption the Pc density of states is broadened while mixing with the bands of the substrate.[19,28,29] Such molecular bending is further enhanced on Al(001), where the central C-H bonds directly interact with the Al atoms underneath. This strong chemical bond, together with the plasticity of the Al substrate gives rise to a V-shaped molecular configuration at most adsorption sites.[21,30] In these cases, the leitmotiv driving the orientation of PAHs on metal surfaces is the maximization of the overlap between aromatic molecular orbitals and surface charge density close to the Fermi level.

In this work we experimentally and theoretically investigate the adsorption of Pc on the (111) surface of Pt. We probe the surface by the means of several experimental techniques, namely scanning tunnelling microscopy (STM), X-ray photoemission spectroscopy (XPS) and near-edge X-ray fine structure (NEXAFS) spectroscopy. We obtain its ground and core-excited states using DFT for several adsorption sites, while accounting for the vdW interaction. We quantify the effect of using various vdW correction methods: from common pairwise corrections to more recent non-local functionals. Furthermore, by comparing STM experimental constant height images and constant current height profiles with the simulated ones, we verify the most probable adsorption configuration: the one in which the molecule lies almost flat on a bridge site, with its long axis parallel to the surface hcp lattice. These results are further corroborated by XPS and NEXAFS spectra which, additionally, indicate the presence of a strong bond at the interface.

Methods

The STM measurements were performed in an ultra high vacuum (UHV) chamber with a base pressure of 10^{-16} mbar, equipped with a commercial apparatus (room temperature Omicron head, driven by Nanotec electronics) at the ESISNA group of the ICMM-CSIC (Madrid). The X-ray Synchrotron radiation experiments were performed at the ALOISA beamline[31] of the ELETTRA synchrotron facility in Trieste (Italy). We employed two different samples in the respective laboratories that were prepared by consolidated UHV cleaning procedure (Ar^+ sputtering at 1-2 kV, followed by annealing to $\sim$1000-1050 K). Eventually, oxygen exposure at 900 K to remove residual carbon followed by hydrogen exposure at 500 K to remove residual oxygen was employed to achieve a chemically pure surface. Pc was evap-

orated at 450-470 K from home-made boron nitride crucibles, while keeping the sample at room temperature. All subsequent measurements were performed at room temperature. For STM experiments, the coverage corresponding to 1 monolayer (ML) was defined through inspection of the first layer of adsorbed molecules at the maximum packing density. In X-ray absorption experiments, the nominal 1 ML was determined by thermal desorption corresponding to an equivalent thickness of 2.5 Å, when monitored with a quartz microbalance. The NEXAFS spectra at the carbon K-edge were measured with the resolution set to ∼80 meV keeping the sample at constant grazing angle of 6°. The orientation of the surface with respect to the photon beam polarization was changed from s-polarization to close to p-polarization by simply rotating the sample coaxial to the photon beam axis. We collected partial electron yield spectra by means of a channeltron equipped with a repelling grid biased to -230 V in order to reject the low energy secondary electrons. Further details about calibration and normalization of the apparatus can be found in Ref.[26]. The XPS spectra of the C 1s excitation were measured with a photon energy of 400 eV (overall resolution of ∼150 meV), while keeping the surface at a grazing angle of 4° in a close to p-polarization and almost normal emission. Surface contamination by oxide species was monitored by XPS with a photon energy of 650 eV (resolution of 280 meV).

The calculations were carried out within the framework of DFT, using Quantum ESPRESSO (QE)[32] distribution. Our simulations were based on the GGA-PBE[33] exchange-correlation functional and on pseudopotentials generated employing the ultrasoft formalism[34] and using the RRKJ[35] recipe. The analysis for convergence showed that the plane wave cutoffs for kinetic energy and charge density of 31 and 321 Ry respectively were sufficient to describe the ground state of the system. The periodically repeated supercell with Pt(111) substrate was made of 7×4 surface unit cells with 14 Å of vacuum region above it. Three layers of Pt atoms were used, of which only the topmost was allowed to relax in order to mimic the bulk behaviour and to reduce the computational load. The Brillouin zone was sampled by an off-Γ 2×3×1 k-points grid that was generated through the Monkhorst-Pack scheme.[36] We additionally verified the relative stability and convergence for the two most stable configurations (namely bri0 and fcc0, as defined in the next section) by considering a slab of six Pt layers, with the top two layers free to relax. The slab was built using the lattice parameter found by the minimization of the energy-volume curve for the bulk phase of Pt. For the case of PBE functional the calculated value was 4.00 Å, while for the vdW non-local functional it was 3.94 Å. For comparison, the experimentally determined value is 3.92 Å.[37] We added the molecule onto only one side of the slab, resulting in an asymmetric design of the supercell. To restore the boundary conditions we added a sawtooth electric field in the middle of the vacuum region, the magnitude of which was calculated from the actual charge density of the system.[38]

The vdW interaction was accounted for by three different approaches, namely, Grimme's D2,[39] the vdW$_{surf}$[40] and the vdW-DF2-C09[41–45] (which we hereafter shorten as vdW$_{nl}$). Charge density dependent calculation of the vdW coefficients (Tkatchenko-Scheffler approach[46]) is not yet fully implemented in QE, hence we performed the vdW$_{surf}$ calculations with Vienna Ab-initio Simulation Package (VASP).[47] For these simulations we used a cutoff of 29 Ry and found the Pt lattice parameter to be 3.97 Å. After relaxing the geometry, all

further post-processing steps, namely computing the electronic DOS and spectra, were done with QE; therefore the atomic coordinates obtained from VASP were slightly stretched to match the value of lattice parameter obtained from QE. We verified however that such procedure had not altered the electronic properties of the system beyond numerical accuracy. For plotting the density of states (DOS), a gaussian smearing was applied with a standard deviation σ of 0.13 eV. The simulated STM data was obtained using the Tersoff-Hamann[48] picture.

We focused on the K-edge energy window in describing the photon absorption process, namely exciting the electrons of the 1s carbon core state. The transition either to an unoccupied bound or to a free-electron state needs to be modelled in different ways. We described the latter by an electronically relaxed calculation employing a pseudopotential with a full hole in the atomic core level (FCH) by the means of the ΔSCF approach[49] in order to obtain the XPS spectrum. In the former case (transition to unoccupied bound state) instead, which gives the NEXAFS spectrum, a half core hole (HCH) pseudopotential is better suited to describe the interaction of the excited electron with the hole it left behind, by the means of the transition potential approach,[50] which is successfully applied to adsorbed systems of increasing size.[51] Calculation of the matrix elements of the transitions was performed using the Xspectra[52] tool of the QE suite, which relies on the Lanczos algorithm[50,53] to avoid simulating all the possible final states. Both HCH and FCH pseudopotentials include all-electron core states reconstruction given by the PAW[54] formalism; and required an higher cutoff of 62 Ry. Since the system, in its entirety, shows a metallic behavior, we assumed a neutral supercell and set the energy reference to the Fermi level. The total spectra were calculated as the average of the ones obtained by selecting the above FCH or HCH pseudopotentials for each inequivalent C atom, weighted by its degeneracy. We constructed the XPS results by broadening the delta-like contributions with pseudo-Voigt profiles with 0.38 eV as gaussian σ, 0.17 eV as the lorentzian width γ and 0.47 as the mixing parameter of the two distributions. These values were obtained by fitting to the experimental data. On the other hand, for the NEXAFS spectra we followed an energy-dependent scheme[55] with a width γ=0.2 eV for energies up to E_F + 5 eV, γ=1 eV for energies higher than E_F + 25 eV and a linear dependence in between, in order to mimic the broadening due to the vibrational spectrum.

Results and Discussion

Adsorption configuration

At low coverage, the Pc molecules can be easily identified in the room temperature STM images as individual straight segments, about 2 nm long, that display the same three-folded azimuthal orientation along the substrate $[10\bar{1}]$, $[01\bar{1}]$, and $[1\bar{1}0]$ (<110>) directions, as shown in Figure 1a. Pc molecules do not display any intermolecular interaction, either attractive or repulsive. In fact, a fully disordered film is observed at a coverage of 1 ML, as shown in Figure 1b, which is indicative of a molecule to substrate interaction much stronger than the intermolecular one. In STM images, we also noticed the occurrence of a few shorter features that display the same azimuthal orientation and intramolecular contrast of pentacene and can be identified with tetracene species. Shorter acene species are normally found as

contaminants of pentacene powder that cannot be easily removed because the surrounding pentacene medium traps these species well beyond their sublimation temperature. There are also a few spot-like feature, the nature of which is more difficult to ascertain because they might be equally associated with benzene or smaller carbonaceous fragments. In any case, we remark that neither tetracene nor the spot-like features display any interaction with the pentacene molecules or among themselves (not even at higher coverage), hence they do not affect the structural and electronic properties of chemisorbed pentacene. At a coverage of 1 ML, small second layer clusters are formed before the completion of the first one. Second layer molecules are easily desorbed at mild temperature (400 K), whereas molecules in the contact layer remains on the surface beyond 1100 K passing through different stages of cyclodehydrogenation and aggregation. The strong sticking of pentacene to platinum is not unexpected, since the Pt(111) surface is well known to yield the formation of graphitic domains starting from adsorbed hydrocarbons.[56] Occasionally, the tip contrast changed and it was possible to observe the Pt atoms underneath by recording the current tunnelling through the molecules. In such cases, as shown in Figure 1c, the molecular footprint indicates that Pc adsorbs atop the surface atom rows along one of the <110> directions, even if it is not possible to discriminate further between on-top and on-bridge sites.

Our calculations focused on the most symmetric configurations as a starting point for the relaxation of ionic coordinates. We evaluated ten configurations (shown in Figure S1 of Electronic Supporting Information, ESI), covering six adsorption sites (namely top, three inequivalent bridge and two hollow sites) and three main azimuthal orientations, namely 0° and ±30°. Each configuration was named after the position of the central aromatic ring and the in-plane azimuthal orientation of the molecular long axis with respect to the $[10\bar{1}]$ direction. For all the simulated systems, we calculated the adsorption energy by subtracting the energy of the clean surface and the one of an isolated molecule from the total energy of the combined system. The most favoured adsorption site is bri0, independent of the vdW correction chosen, i.e. the central hexagon of pentacene has the same adsorption site and orientation as reported for benzene,[14] although the latter configuration is defined with a different nomenclature. In fact, the azimuthal orientation of benzene with respect to the $[10\bar{1}]$ direction is referenced to the C-C diagonal, which is at 30° from the long molecular axis for a hexagon in the pentacene molecule. However the hierarchy of the other configurations in the energy landscape depends on the vdW term. For the sake of simplicity we will hereafter only discuss the adsorption sites that yielded the two highest adsorption energies, namely bri0 and fcc0. In addition, we will also address the top0 configuration, which is the only remaining one that is compatible with the molecular orientation observed in STM images. In fact, the aforementioned through-molecule STM images point to exclude the fcc0 geometry, which was however reported to be the adsorption site on Cu(111).[57]

In Figure 3 we compare the adsorption energies for the bri0, fcc0 and top0 configurations, by applying different vdW correction schemes. The adsorption energy obtained for Pc (five linearly-fused benzene rings) from PBE, without the inclusion of vdW corrections, is small (3.13 eV) considering that the adsorption energy measured for a single Bz molecule is 1.9 eV, showing that the dispersion interactions are crucial for calculating more accurate values. On comparing different dispersion correction methods, the D2 method yields systematically

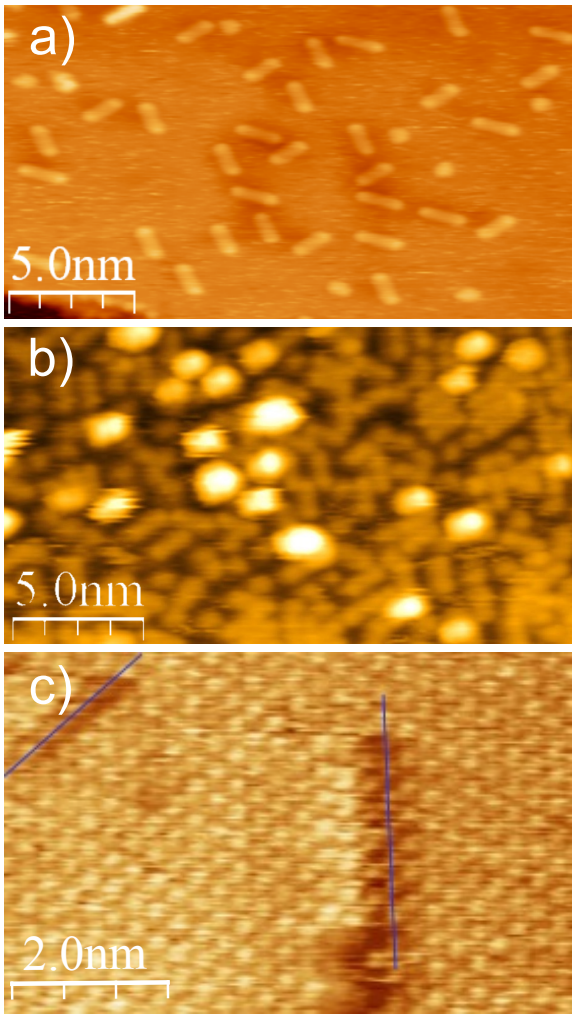

Figure 1: Experimental STM images of Pc on Pt(111). The panels a) and b) show low and high (∼1ML) coverage samples, respectively (sample bias 1 V and 1.5 V, respectively, 25 nm × 12.6 nm); no molecular aggregation is observed in the contact layer and small second layer clusters are observed at a coverage of 1 ML, before the completion of the first one. c) Tunnelling-enhanced image close-up of isolated molecules showing also the atoms of the substrate (sample bias 0.5 V).

larger energies than those obtained from the other two methods, which seems to be a result of the large C_6 coefficient assigned to Pt when using Grimme's technique.[58] On the other hand, the results calculated with the vdW$_{nl}$ approach and with vdW$_{surf}$ method are comparable with each other. The results for the other configurations are addressed in Tables S1 and S2. Since the molecule distorts upon adsorption, the carbon atoms in the Pc molecule are forced into two roughly planar regions defined by the highest-lying and the lowest-lying C atom respectively, and separated by a distance Δz. The adsorption height z is then defined as the difference between averaged z coordinates of atoms in the lower region and the averaged z coordinates of the Pt atoms in the topmost layer. The adsorption height z, the distortion of molecular geometry Δz and the adsorption configurations are all reported in Figure 3. For the most stable configuration (bri0) the geometry is almost the same for all tested vdW corrections. A similar adsorption height is found for the other adsorption sites as well, however the shape of the molecule varies from case to case. These results are reported in Table S3.

The adsorbed molecule may assume two distinct configurations: showing a concave distortion at the bridge sites and a convex distortion at the top as well as hollow sites. The difference is driven by the correspondence between the position of the aromatic rings and the substrate atoms. In analogy with the case of benzene,[14] the aromatic carbon rings at top sites are the least stable ones and are therefore less bound to the surface and vice-versa for bridge sites. The deformation energy required for the molecular distortion is the origin of the difference in the adsorption energy. We also note that the surface is slightly buckled, with atomic displacements along the normal to the surface up to 8% of the bulk Pt-Pt distance; for the bri0 configuration this effect is visualised in Figure S2 of ESI.

The adsorption molecular conformation obtained from simulations is very similar to what has been observed on the Cu(111) surface,[29] but at a different adsorption site (namely fcc0) and with a larger adsorption energy. In particular, although the extent of molecular distortion is the same as that for Pc on copper,[29] an adsorption height of $\sim$2.0 Å on Pt(111) is smaller than on Cu(111) where the experimentally measured height ($\sim$2.34 Å)[59] was consistent with the theoretical result.[29] Conversely, on the most reactive orientation Cu(110), a vertical height close to 2 Å was reported for the two central carbon atoms.[27] This is however accompanied by a larger molecular distortion (0.8 Å[19]). Overall, the close proximity of Pc to Pt(111) surface is the first indication of a strong molecule-metal interaction.
The large value calculated for the binding energy and the short adsorption distance both suggest that the interaction may be so strong as to form chemical bonds between carbon atoms and platinum surface. The adsorption geometry corroborates this idea: a C atom rearranging the electronic orbitals from an sp^2 to an sp^3 hybridization should display a tetrahedron-like geometry with the surrounding atoms. Within this picture, the angle formed between H-C-Pt atoms should be as close to 109° for it to be in sp^3 hybridization. Indeed, in the bri0 configuration these angles are $\sim$102° with respect to the nearest Pt atom.

Electronic properties

High intramolecular resolution was achieved in STM imaging due to low mobility of the adsorbed molecules, as seen in the false color image shown in Figure 2a. The simulations of

the intra-molecular contrast and of the vertical profile of Pc molecule on Pt(111), as shown in Figure 2, consistently support a slightly concave geometry. On the contrary, hollow and top sites display the same deformation that is of the convex type, as depicted in Figure 3. This conformation is not compatible with the experimental data, as shown in Fig. S4 (ESI) for the specific case of the fcc0 hollow site. For comparison, the same molecular profile as

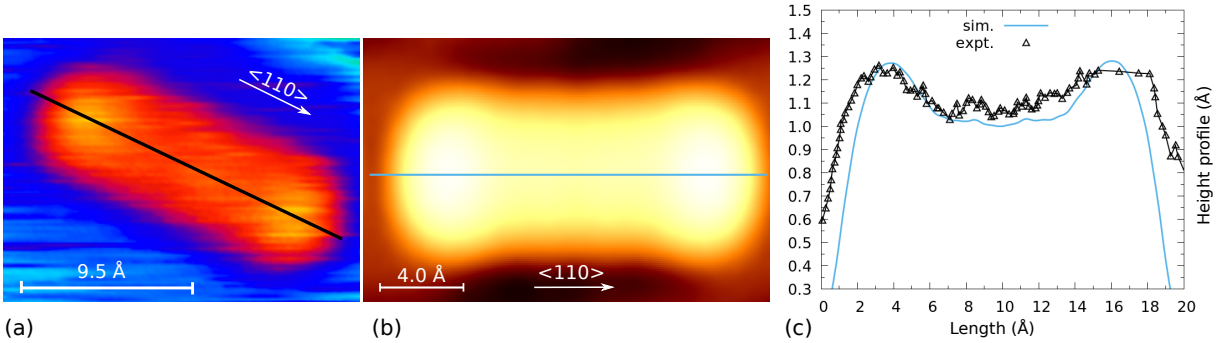

Figure 2: STM images and height profiles. Panels a) and c) show the experimental results (0.5 V sample bias and 0.396 nA tunnelling current), while panels b) and c) reports the simulated ones for the bri0 configuration.

obtained here for the bridge site was instead reported for Pc adsorbed on Cu(111) at the hollow fcc0 one.[29,57]

Upon adsorption, the molecule looses its electronic gas-phase properties and the correspondence with the molecular orbitals (MO) is lost (no nodal planes are detected). In order to highlight the charge displacement, we calculated the difference in the charge density between the adsorbed and the isolated systems $\Delta\rho = \rho_{Pc/Pt} - \rho_{Pc} - \rho_{Pt}$, which is shown as charge accumulation/depletion lobes in Figure 3. Performing a Löwdin population analysis[60] on the bri0 configuration, as obtained with the vdW$_{surf}$ correction, we estimated that 1.5 electrons are transferred from the metal to the Pc. This value is significantly larger than the 0.8 e$^-$ value reported for adsorption on the most reactive orientation (110) of copper.[19] For an estimate of the charge transfer at other adsorption sites, please refer to table S2. In all the adsorption configurations of interest we observed the largest modification of the electronic charge density in the region between the first layer of the surface and the molecule, specifically in correspondence with every carbon atom that is also coordinated to a Pt atom underneath, which is indicative of the establishment of C-Pt bonds. As expected, the Pt atom buckling is accompanied by charge rearrangement below the most displaced atoms, i.e. those directly coordinated to the carbon atoms. We simulated the DOS (for the bri0 site, but similar results are obtained for the other configurations); its projections onto the gas phase MO shows a metallic behaviour and the hybridization with the bands of the substrate. as reported and further discussed with Figure S3 (ESI).

In general, assigning interactions at the interface to physisorption or chemisorption is not straightforward.[6,19] However, we have pointed out several effects, namely adsorption configuration (including the substrate distortion), charge transfer and mixing of the electronic

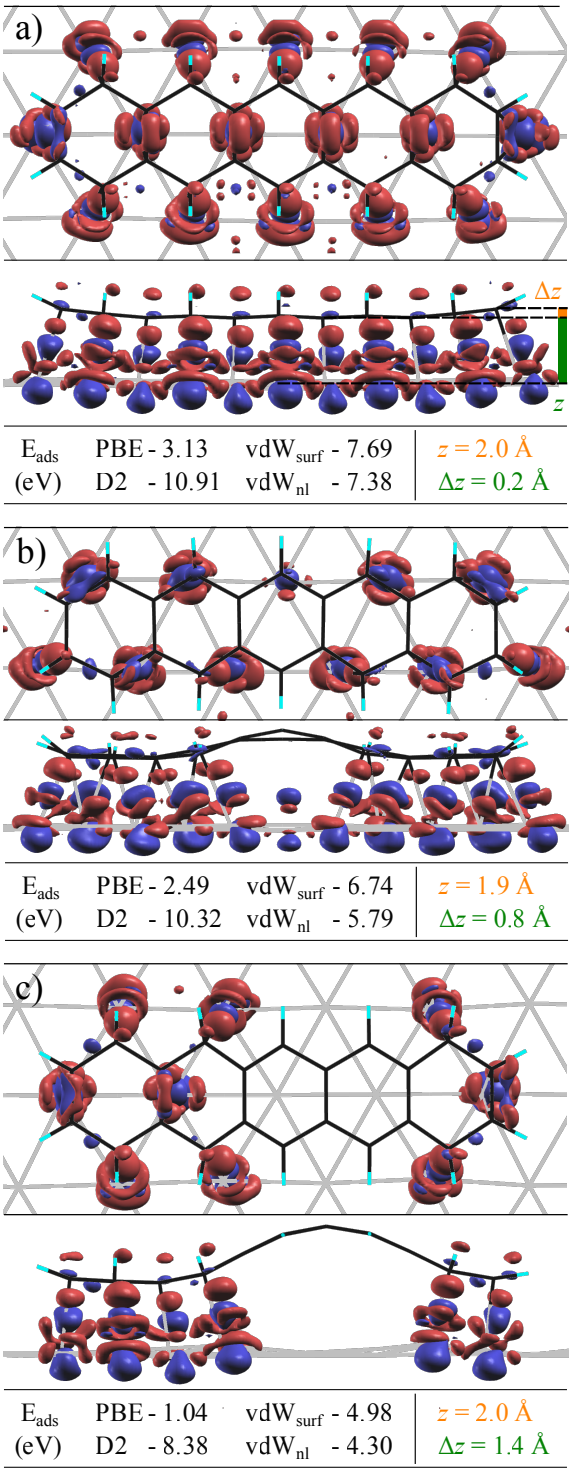

Figure 3: Adsorption geometry and $\Delta\rho$ for the configurations of interest calculated with vdW$_{surf}$: a) bri0, b) fcc0, c) top0. The red lobes show e$^-$ accumulation, the blue ones the depletion areas. The isosurfaces correspond to the value of 0.01 e/Bohr^3.

states, all of which identify the adsorption process as driven by non-dissociating chemical reactions. These results agree with those obtained for Pc on Cu substrate.[19,28] The same behaviour is observed also for simulations at the hollow and top sites, which consistently indicates that here the chemisorption is driven by the specific reactivity of Pt substrate, in full agreement with the observed persistency of pentacene beyond the set in temperature of cyclo-dehydrogenation.

X-ray spectroscopy

We analysed the Pc adsorption on Pt(111) by synchrotron radiation photoemission and absorption spectroscopy, the former technique yielding the charged state of the molecule, the latter one probing the unoccupied molecular orbitals and, hence, the charge transfer from the substrate.

The experimental XPS spectrum is reported in Figure 4 for a nominal coverage of 1 monolayer (ML), after an annealing step at 400 K. In fact, even if the annealing does not yield any

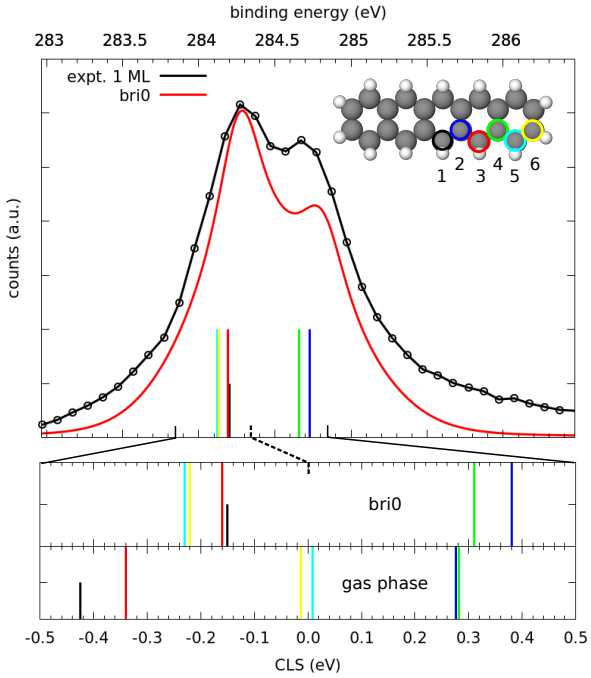

Figure 4: Experimental and simulated XPS results. The lower panel shows the comparison between the CLS for gas phase and after the adsorption. The simulated spectrum is shifted to align its strongest excitation peak with the experimental one at 284.25 eV.

long range ordered molecular aggregation, it effectively desorbs the molecules beyond the 1st layer (that are observed in Figure 1b before the completion of the first layer) and favours a more homogeneous surface wetting. This improves the degree of orientational order, thus allowing a better comparison with the case of the isolated molecule, as measured by STM and simulated by DFT (see spectroscopic data in Figures S7 and S8 of ESI). The energy is reported as binding energy (BE) with respect to the Fermi level, while in our simulated XPS we

refer the core level shifts (CLS) to the total energy averaged among the inequivalent C atoms.

We may resolve two main peaks around 284.5 eV and an asymmetric background signal that can be associated with multiple satellites in the peak tail at high binding energy.[61] We seldom observed a broad weak shoulder at 286 eV of varying intensity (depending on the deposition conditions and substrate temperature), which can be associated with adventitious carbon contamination (e.g. CO[62]) originated by the heating filament of the crucible. In fact, the shoulder at 286 eV disappears upon mild annealing at 400 K together with a small oxygen peak that is formed after the deposition at RT (see Figure S7, ESI). The split shape of the main component at ∼284.5 eV is much different from that reported on gold,[18] the latter being quite similar to the gas phase one.[63,64] In particular, the 0.5 eV peak splitting is the same as observed for Pc on copper surfaces,[65,66] even if with reversed relative intensity of the main components, which rather resemble the shape reported for aluminium.[30] This spectroscopic evidence is also indicative of a strong chemical interaction with the substrate. Our XPS results show a good agreement between the experimental spectrum and the one calculated for the bri0 configuration, thus supporting our previous observations about the adsorption configuration. By looking at the calculated CLS, we may distinguish two kinds of bonds. The one at lower BE due to H-bonded C atoms, while the other one due to C-C bonds. In the bri0 geometry the C atoms labelled 1,3,5,6 show closer contributions than in gas phase, suggesting that the electronic states may be divided into sp^2 (C atoms labelled 2 and 4 in Figure 4) and almost-sp^3 configurations (C atoms labelled 1, 3, 5 and 6). Because of the overall small molecular distortion, the chemical configuration (initial state) dominates the hierarchy of the binding energy with respect to final state effects, such as the charge screening of the core-hole by the metal Fermi electrons, the strength of which depends on the local distance of the C atom from the surface. For comparison, simulations performed for the fcc0 and top0 configurations (the former is reported in Figure S5, ESI) yield a much different XPS profile, due to their different bonding scheme and convex shape. As a consequence, the DFT calculations as well as both STM and XPS results, all consistently point to the same slightly concave adsorption configuration found at the bri0 site.

The NEXAFS spectra for the 1 ML film after annealing at 400 K, reported in Figure 5, show a polarization-dependent intensity. Such a dichroic effect has been observed previously;[63,64] however, because of the strong hybridization of the electronic levels, the individual gas phase MO contributions cannot be associated any longer with any specific resonance, rather they are merged into one large band. By calculating the NEXAFS spectrum for each inequivalent C atom (see Figure S6 of ESI), we observe that atoms C1, C3 and C5 contribute less to the feature at 287 eV when compared to other carbon atoms. At all other resonances, all carbon atoms contribute evenly to the main NEXAFS spectra. Overall, the simulated results correctly reproduce the energy position of the main peaks both below and above the ionization threshold. Only a minor discrepancy is found for the relative intensities of the two largest features at ∼285.5 and 287 eV. In particular, the first peak is flanked on the high energy side by a component that originates either from residual 2nd layer molecules (as suggested by the comparison with the multilayer spectra shown in Figure S8, ESI) or from residual contaminants (molecular fragments) produced during the deposition, as observed in the STM images. We can exclude the origin of this contribution from oxidized carbon

species, because oxygen is entirely removed from the surface after mild annealing to 400 K (see XPS spectra in Figure S7 of ESI).

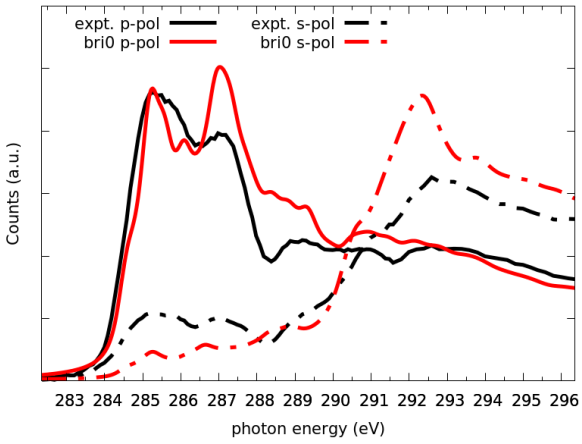

Figure 5: Comparison of the experimental NEXAFS spectra measured at 1 ML (after annealing to 130°C) with the simulated ones for the most stable configuration (bri0). The simulated spectra are shifted in order to align with the experimental feature observed at 287.2 eV. The simulated NEXAFS spectra are rescaled to match the experimental NEXAFS intensity above the ionization threshold.

Conclusion

We have combined experimental and theoretical techniques to investigate the hybrid metal-organic Pc/Pt(111) system. In order to understand the nature of the molecule-substrate interaction, we also performed a systematic evaluation of multiple adsorption configurations based on energetics and correspondence with experiments. The molecules are found to adsorb uniquely at bridge sites atop the close-compact Pt rows with their long axis oriented along the <110> surface directions. Additionally, the two ends of Pc molecules display small upward bending (Δz ~0.2 Å). We did not find any evidence of molecular aggregation in ordered/oriented domains. Although the adsorption configuration of molecules (deformation and azimuthal orientation) resembles that reported for pentacene on different copper surfaces, the adsorption site on Pt(111) is different from the one reported for Cu(111). Also, the Löwdin charge population analysis indicates a charge transfer of 1.5 e^- from the substrate to the molecule, which is almost twice that reported in the case of copper. From our analysis of results of DFT simulations as well as STM, XPS and NEXAFS measurements we consistently conclude that pentacene is in a chemisorbed state which is induced mainly by the reactivity of Pt. We see that there is a relatively good match between the molecular carbon backbone and the substrate lattice spacing. This allows all H-bonded C atoms to bond with a Pt atom underneath in a close sp^3 geometry without significant distortions in the molecule. The strong adsorption regime disrupts the gas-phase electronic properties of the molecule and results in metallic and hybridized features.

Acknowledgement

This work was performed in the PCAM network of European doctorate. S.S.H. acknowledges support from the European Union Seventh Framework Programme under grant agreement number 607232 (THINFACE). L.F. acknowledges financial support from CNR-INFN national project (PREMIALE 2012) EOS 'Organic Electronics for Innovative research instrumentation'. ESISNA group acknowledge funding from MAT2014-54231-C4-1-P.

Supporting Information Available

Detailed adsorption energy and adsorption geometry results for all the simulated configurations as well as their comparison for different vdW correction methods, the calculated density of states, the simulated STM and XPS results for the second most stable configuration, NEXAFS spectrum of each inequivalent C atom and a note on the coverage-dependence of experimental results are available.

References

(1) Kronik, L.; Koch, N. Electronic properties of organic-based interfaces. MRS Bull. **2010**, 35, 417–422.

(2) Anthony, J. E. Functionalized acenes and heteroacenes for organic electronics. Chem. Rev. **2006**, 106, 5028–5048.

(3) Kymissis, I. Organic Field Effect Transistors: Theory, Fabrication and Characterization; Springer US, 2009.

(4) Koch, N. Organic electronic devices and their functional interfaces. ChemPhysChem **2007**, 8, 1438–1455.

(5) Hwang, J.; Wan, A.; Kahn, A. Energetics of metal-organic interfaces: New experiments and assessment of the field. Mater. Sci. Eng. R Reports **2009**, 64, 1–31.

(6) Koch, N. Energy levels at interfaces between metals and conjugated organic molecules. J. Phys. Condens. Matter **2008**, 20, 184008.

(7) Nausieda, I.; Ryu, K. K.; He, D. D.; Akinwande, A. I.; Bulovic, V.; Sodini, C. G. Dual threshold voltage organic thin-film transistor technology. IEEE Trans. Electron Devices **2010**, 57, 3027–3032.

(8) Tsamados, D.; Cvetkovic, N. V.; Sidler, K.; Bhandari, J.; Savu, V.; Brugger, J.; Ionescu, A. M. Double-gate pentacene thin-film transistor with improved control in sub-threshold region. Solid. State. Electron. **2010**, 54, 1003–1009.

(9) Bond, B. G. C. Periodic variations in the catalytic properties of metals. Platin. Met. Rev. **2005**, 12, 100–105.

(10) Klimeš, J.; Michaelides, A. Perspective: Advances and challenges in treating van der Waals dispersion forces in density functional theory. J. Chem. Phys. **2012**, 137, 120901.

(11) Hohenberg, P.; Kohn, W. Inhomogeneous electron gas. Phys. Rev. **1964**, 864.

(12) Kohn, W.; Sham, L. J. Self-consistent equations including exchange and correlation effects. Phys. Rev. **1965**, A1133–A1138.

(13) Zhang, R.; Hensley, A. J.; McEwen, J.-S.; Wickert, S.; Darlatt, E.; Fischer, K.; Schöppke, M.; Denecke, R.; Streber, R.; Lorenz, M. et al. Integrated X-ray photoelectron spectroscopy and DFT characterization of benzene adsorption on Pt(111), Pt(355) and Pt(322) surfaces. Phys. Chem. Chem. Phys. **2013**, 15, 20662–20671.

(14) Ayishabi, P.; Lakshmikanth, K.; Chatanathodi, R. Chemisorption of benzene on Pt (111) surface: A DFT study with van der Waals interaction. Chem. Phys. Lett. **2015**, 637, 182–188.

(15) Liu, W.; Ruiz, V. G.; Zhang, G. X.; Santra, B.; Ren, X.; Scheffler, M.; Tkatchenko, A. Structure and energetics of benzene adsorbed on transition-metal surfaces: Density-functional theory with van der Waals interactions including collective substrate response. New J. Phys. **2013**, 15.

(16) Yildirim, H.; Greber, T.; Kara, A. Trends in Adsorption Characteristics of Benzene on Transition Metal Surfaces: Role of Surface Chemistry and van der Waals Interactions. J. Phys. Chem. C **2013**, 117, 20572–20583.

(17) Ihm, H.; Ajo, H. M.; Gottfried, J. M.; Bera, P.; Campbell, C. T. Calorimetric measurement of the heat of adsorption of benzene on Pt(111). J. Phys. Chem. B **2004**, 108, 14627–14633.

(18) Floreano, L.; Cossaro, A.; Cvetko, D.; Bavdek, G.; Morgante, A. Phase diagram of pentacene growth on Au(110). J. Phys. Chem. B **2006**, 110, 4908–4913.

(19) Muller, K.; Seitsonen, A. P.; Brugger, T.; Westover, J.; Greber, T.; Jung, T.; Kara, A. Electronic structure of an organic/metal interface: Pentacene/Cu(110). J. Phys. Chem. C **2012**, 116, 23465–23471.

(20) Käfer, D.; Witte, G. Evolution of pentacene films on Ag(1 1 1): Growth beyond the first monolayer. Chem. Phys. Lett. **2007**, 442, 376–383.

(21) Baby, A.; Lin, H.; Brivio, G. P.; Floreano, L.; Fratesi, G. Core-level spectra and molecular deformation in adsorption : V-shaped pentacene on Al (001). Beilstein J. Nanotechnol. **2015**, 6, 2242–2251.

(22) Kang, J. H.; Zhu, X. Y. Layer-by-layer growth of incommensurate, polycrystalline, lying-down pentacene thin films on Au(111). Chem. Mater. **2006**, 18, 1318–1323.

(23) France, C. B.; Schroeder, P. G.; Parkinson, B. a. Direct observation of a widely spaced periodic row structure at the pentacene/Au(111) interface using scanning tunneling microscopy. Nano Lett. **2002**, 2, 693–696.

(24) Casalis, L.; Danisman, M.; Nickel, B.; Bracco, G.; Toccoli, T.; Iannotta, S.; Scoles, G. Hyperthermal molecular beam deposition of highly ordered organic thin films. Phys. Rev. Lett. **2003**, 90, 18–21.

(25) Wang, Y.; Ji, W.; Shi, D.; Du, S.; Seidel, C.; Ma, Y.; Gao, H.-J.; Chi, L.; Fuchs, H. Structural evolution of pentacene on a Ag(110) surface. Phys. Rev. B **2004**, 69, 1–5.

(26) Bavdek, G.; Cossaro, A.; Cvetko, D.; Africh, C.; Blasetti, C.; Esch, F.; Morgante, A.; Floreano, L.; Tasc, C.-i. L. N.; Ss, B. et al. Pentacene Nanorails on Au (110). Langmuir **2008**, 767–772.

(27) Sauvage-Simkin, M.; Coati, A.; Garreau, Y.; Vlad, A.; Müller, K.; Bendounan, A.; Kara, A. In-depth atomic structure of the pentacene/Cu(110) interface in the monolayer coverage regime: Theory and x-ray diffraction results. J. Phys. Chem. C **2014**, 118, 27815–27822.

(28) Ferretti, A.; Baldacchini, C.; Calzolari, A.; Di Felice, R.; Ruini, A.; Molinari, E.; Betti, M. G. Mixing of electronic states in pentacene adsorption on copper. Phys. Rev. Lett. **2007**, 99, 1–4.

(29) Shi, X. Q.; Li, Y.; Van Hove, M. A.; Zhang, R. Q. Interactions between organics and metal surfaces in the intermediate regime between physisorption and chemisorption. J. Phys. Chem. C **2012**, 116, 23603–23607.

(30) Baby, A.; Fratesi, G.; Vaidya, S. R.; Patera, L. L.; Africh, C.; Floreano, L.; Brivio, G. P. Anchoring and bending of pentacene on aluminum (001). J. Phys. Chem. C **2015**, 119, 3624–3633.

(31) Floreano, L.; Cossaro, A.; Gotter, R. Periodic arrays of Cu-phthalocyanine chains on Au (110). J. Phys. Chem. C **2008**, 10794–10802.

(32) Giannozzi, P.; Baroni, S.; Bonini, N.; Calandra, M.; Car, R.; Cavazzoni, C.; Ceresoli, D.; Chiarotti, G. L.; Cococcioni, M.; Dabo, I. et al. QUANTUM ESPRESSO: a modular and open-source software project for quantum simulations of materials. J. Phys. Condens. Matter **2009**, 21, 395502.

(33) Perdew, J. P.; Burke, K.; Ernzerhof, M. Generalized Gradient Approximation made simple. Phys. Rev. Lett. **1996**, 77, 3865–3868.

(34) Vanderbilt, D. Soft self-consistent pseudopotentials in a generalized eigenvalue formalism. Phys. Rev. B **1990**, 41, 7892–7895.

(35) Rappe, A. M.; Rabe, K. M.; Kaxiras, E.; Joannopoulos, J. D. Optimized pseudopotentials. Phys. Rev. B **1990**, 41, 1227–1230.

(36) Methfessel, M.; Paxton, A. T. High-precision sampling for Brillouin-zone integration in metals. Phys. Rev. B **1989**, 40, 3616–3621.

(37) Wyckoff, R. W. G. Crystal structures; John Wiley: New York, 1963.

(38) Bengtsson, L. Dipole correction for surface supercell calculations. Phys. Rev. B **1999**, 59, 12301–12304.

(39) Grimme, S. Semiempirical GGA-type density functional constructed with a long-range dispersion correction. J. Comput. Chem. **2006**, 27, 1787–1799.

(40) Ruiz, V. G.; Liu, W.; Zojer, E.; Scheffler, M.; Tkatchenko, A. Density-functional theory with screened van der Waals interactions for the modeling of hybrid inorganic-organic systems. Phys. Rev. Lett. **2012**, 108, 2–6.

(41) Thonhauser, T.; Cooper, V. R.; Li, S.; Puzder, A.; Hyldgaard, P.; Langreth, D. C. Van der Waals density functional: Self-consistent potential and the nature of the van der Waals bond. Phys. Rev. B **2007**, 76, 1–11.

(42) Thonhauser, T.; Zuluaga, S.; Arter, C. A.; Berland, K.; Schröder, E.; Hyldgaard, P. Spin signature of nonlocal correlation binding in metal-organic frameworks. Phys. Rev. Lett. **2015**, 115, 1–6.

(43) Berland, K.; Cooper, V. R.; Lee, K.; Schröder, E.; Thonhauser, T.; Hyldgaard, P.; Lundqvist, B. I. van der Waals forces in density functional theory: The vdW-DF method. Reports Prog. Phys. **2015**, 78, 066501.

(44) Langreth, D. C.; Lundqvist, B. I.; Chakarova-Käck, S. D.; Cooper, V. R.; Dion, M.; Hyldgaard, P.; Kelkkanen, A.; Kleis, J.; Kong, L.; Li, S. et al. A density functional for sparse matter. J. Phys. Condens. Matter **2009**, 21, 084203.

(45) Cooper, V. R. Van der Waals density functional: An appropriate exchange functional. Phys. Rev. B **2010**, 81, 1–4.

(46) Tkatchenko, A.; Scheffler, M. Accurate molecular van der Waals interactions from ground-state electron density and free-atom reference data. Phys. Rev. Lett. **2009**, 102, 6–9.

(47) Kresse, G.; Furthmüller, J. Efficient Iterative Schemes for ab initio Total-Energy Calculations Using a Plane-Wave Basis Set. Phys. Rev. B **1996**, 11169–11186.

(48) Tersoff, J.; Hamann, D. R. Theory of the scanning tunneling microscope. Phys. Rev. B **1985**, 31, 805–813.

(49) García-Gil, S.; García, A.; Ordejón, P. Calculation of core level shifts within DFT using pseudopotentials and localized basis sets. Eur. Phys. J. B **2012**, 85.

(50) Slater, J. C.; Johnson, K. H. Self-consistent-field Xα cluster method for polyatomic molecules and solids. Phys. Rev. B **1972**, 5, 844–853.

(51) Diller, K.; Maurer, R.; Müller, M.; Reuter, K. Interpretation of x-ray absorption spectroscopy in the presence of surface hybridization. J. Chem. Phys. **2017**, 146, 214701.

(52) Gougoussis, C.; Calandra, M.; Seitsonen, A. P.; Mauri, F. First-principles calculations of x-ray absorption in a scheme based on ultrasoft pseudopotentials: From α-quartz to high-Tc compounds. Phys. Rev. B **2009**, 80, 1–8.

(53) Lanczos, C. Solution of systems of linear equations by minimized iterations. J. Res. Natl. Bur. Stand. (1934). **1952**, 49, 33.

(54) Blöchl, P. E. Projector augmented-wave method. Phys. Rev. B **1994**, 50, 17953–17979.

(55) Leetmaa, M.; Ljungberg, M. P.; Lyubartsev, A.; Nilsson, A.; Pettersson, L. G. M. Theoretical approximations to X-ray absorption spectroscopy of liquid water and ice. J. Electron Spectros. Relat. Phenomena **2010**, 177, 135–157.

(56) Land, T. A.; Michely, T.; Behm, R. J.; Hemminger, J. C.; Comsa, G. Direct observation of surface reactions by scanning tunneling microscopy: Ethylene $\rightarrow$ Ethylidyne $\rightarrow$ carbon particles $\rightarrow$ graphite on Pt(111). J. Chem. Phys. **1992**, 6774–6783.

(57) Lagoute, J.; Kanisawa, K.; Fölsch, S. Manipulation and adsorption-site mapping of single pentacene molecules on Cu(111). Phys. Rev. B **2004**, 70, 1–6.

(58) Tarball of the current versions of the code and coefficient file (V3.2 Rev 0) located at the Homepage of the Mulliken Center for Theoretical Chemistry. `http://www.thch.uni-bonn.de/tc/downloads/DFT-D3/data/dftd3.tgz`, Accessed: 2017-06-30.

(59) Koch, N.; Gerlach, A.; Duhm, S.; Glowatzki, H.; Heimel, G.; Vollmer, A.; Sakamoto, Y.; Suzuki, T.; Zegenhagen, J.; Rabe, J. P. et al. Adsorption-induced intramolecular dipole: Correlating molecular conformation and interface electronic structure. J. Am. Chem. Soc. **2008**, 130, 7300–7304.

(60) Löwdin, P.-O. On the Nonorthogonality Problem. Adv. Quantum Chem. **1970**, 5, 185–199.

(61) Rocco, M. L. M.; Haeming, M.; Batchelor, D. R.; Fink, R.; Schöll, A.; Umbach, E. Electronic relaxation effects in condensed polyacenes: A high-resolution photoemission study. J. Chem. Phys. **2008**, 129.

(62) Toyoshima, R.; Yoshida, M.; Monya, Y.; Suzuki, K.; Amemiya, K.; Mase, K.; Mun, B. S.; Kondoh, H. A high-pressure-induced dense CO overlayer on a Pt(111) surface: a chemical analysis using in situ near ambient pressure XPS. Phys. Chem. Chem. Phys. **2014**, 16, 23564–23567.

(63) Alagia, M.; Baldacchini, C.; Betti, M. G.; Bussolotti, F.; Carravetta, V.; Ekström, U.; Mariani, C.; Stranges, S. Core-shell photoabsorption and photoelectron spectra of gas-phase pentacene: Experiment and theory. J. Chem. Phys. **2005**, 122.

(64) Fratesi, G.; Lanzilotto, V.; Floreano, L.; Brivio, G. P. Azimuthal dichroism in near-edge X-ray absorption fine structure spectra of planar molecules. J. Phys. Chem. C **2013**, 117, 6632–6638.

(65) McDonald, O.; Cafolla, A. A.; Li, Z.; Hughes, G. Synchrotron photoemission studies of pentacene films on Cu(1 1 0). Surf. Sci. **2006**, 600, 1909–1916.

(66) Baldacchini, C.; Allegretti, F.; Gunnella, R.; Betti, M. G. Molecule-metal interaction of pentacene on copper vicinal surfaces. Surf Sci. **2007**, 601, 2603–2606.

Graphical TOC Entry